Monthly Notices of the ROYAL ASTRONOMICAL SOCIETY

MNRAS **512,** 2402–2407 (2022) https://doi.org/10.1093/mnras/stac554
Advance Access publication 2022 March 3

Lucky imaging speckle statistics applied to halo suppression

Manuel P. Cagigal,[1]★ Pedro J. Valle,[1] Vidal F. Canales [1]★ and Miguel A. Cagigas[2]

[1]*Departamento de Física Aplicada, Universidad de Cantabria, Avenida de los Castros 48, E-39005 Santander, Spain*
[2]*Instituto Astrofísico de Canarias, Vía Láctea S/N, E-38200 La Laguna, Spain*

Accepted 2022 February 25. Received 2022 February 25; in original form 2022 February 10

ABSTRACT

In ground based astronomy, the Lucky Imaging (LI) technique consists of selecting the best quality pictures among those that have been taken with a short exposure time to freeze the atmosphere distortions. Although it has different advantages, the peak intensity of a star is always surrounded by speckled light which, once averaged, provides the halo. The halo can make it difficult to detect faint companions immersed in it. In this paper, we take advantage of the speckle statistics to remove the halo and so to make more effective current detection techniques. Theoretical predictions are confirmed using experimental LI data. Finally, a photometry algorithm is also proposed.

Key words: methods: statistical – telescopes – planets and satellites: detection.

1 INTRODUCTION

Various techniques, such as speckle interferometry (Weigelt & Wirnitzer 1983) and adaptive optics (AO; Hardy 1998), have been used to mitigate the effects of atmospheric refractive index fluctuations on the angular resolution of ground-based telescope images. An alternative technique, suggested by Fried (1978) and called lucky imaging (LI) consists in detecting a series of short-exposure images and then selecting the best of these. The LI technique appears to be very useful because of its low complexity, low costs in terms of hardware, and because it works with reference stars weaker than those required for the AO technique. A key parameter when using LI is the image exposure time, which should approach the atmospheric de-correlation time-scale, which is approximately 30 ms (Mackay 2013).

The image of a point source (the point spread function, PSF) obtained by a perfect clear-pupil optical system can be described by the Airy pattern. However, in ground-based telescopes where atmospheric refractive index inhomogeneities slightly distorts the incoming wave-front, a short exposure image produces a central peak, that is created by the coherent part of the wave-front, surrounded by a number of speckles due to incoherent incoming energy. The shape of the distorted PSF will depend on D/r_0, the ratio between the telescope diameter D and the Fried parameter r_0, which is the atmospheric coherence length. The number of speckles surrounding the central peak is roughly given by $(D/r_0)^2$ and these are randomly distributed over an area with angular diameter λ/r_0. The number of speckles and the area covered by them are strongly dependent on the wavelength λ since r_0 scales with the detection wavelength (or band).

To apply LI we have to detect a large number of images and then to select the best ones. Although different criteria can be applied (Hormuth et al. 2008), we shall select those images with a higher peak intensity, or Strehl ratio. A proper image selection can only be carried out when the height of the coherent peak is approximately twice that of the speckle mean intensity; that is, when $D/r_0 < 8$ (Cagigal et al. 2016). This condition is fulfilled for a telescope with a diameter of up to 2.5 m, when observed in the I-band (700–800 nm wavelength). Finally, we recentre and average the selected images to obtain a sharp image. This image consists of a central peak surrounded by a halo, which comes from the averaged speckles. To observe possible close faint companions, it is mandatory to remove the halo of light by applying a high-pass filter (Hormuth et al. 2008) or by using the COELI covariance algorithm (Cagigal et al. 2016, 2017). The COELI technique is based on the fact that the intensity of pixels where there is a companion fluctuates in phase with the intensity of the main star and the intensity of incoherent speckles fluctuates in counter phase. If we evaluate the covariance between the intensity of the main star pixel and that of the remaining pixels throughout the LI cube, we obtain a 2D covariance map such that pixels where there is a companion will show the highest covariance value. This technique has been successfully applied in order to reduce the speckled background in a region around the host star with an inner radius of $1.22\ \lambda/D$ and outer radius of $1.22\ \lambda/r_0$ (Cagigal et al. 2016, 2017).

In this paper, we introduce a procedure to reduce the speckle halo in the LI cube that allows both techniques, high-pass filtering and COELI processing, to achieve better results. We take advantage of light speckle statistics to remove, or at least reduce, the halo's contribution to the final image. We first analyse experimental speckle statistics in LI images and then use a Rician distribution to describe it. We estimate the standard deviation (STD) of the speckle intensity within the halo in different ways and we use this information to reduce the halo weight in the final image. We have also checked that the signal-to-noise ratio (SNR) of the images may also give us valuable information about the presence of companions. Finally, we have introduced a section to describe a procedure to obtain approximate photometry of the image.

★ E-mail: perezcm@unican.es (MPC); fernancv@unican.es (VFC)

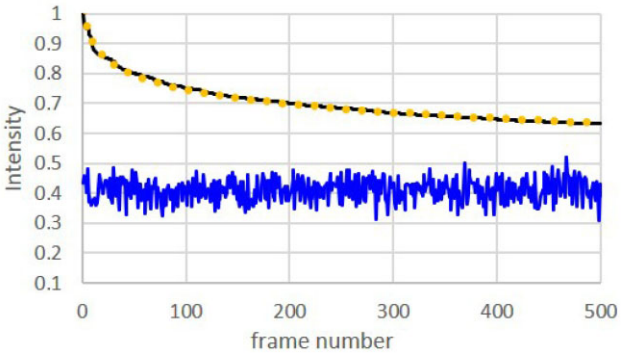

Figure 1. Normalized peak intensity throughout the cube frames (black line), logarithmic fitting curve (yellow dotted line), and normalized intensity of a pixel within the halo throughout the cube frames (blue line).

2 SHORT-EXPOSURE IMAGE STATISTICS

2.1 Peak series behaviour

For a perfectly flat wave-front, the central peak shape of a short-exposure image is described by the Airy pattern, assuming a circular aperture. Its height, which depends on the coherent energy in the incoming wave-front, will decrease as the wave-front becomes more distorted. In an LI experiment, those frames with a higher central peak are chosen and then sorted in decreasing order. Fig. 1 shows the typical behaviour of the normalized peak intensity (black line) throughout an experimental image series of 500 frames. We also show, with a yellow dotted line, the fitting line corresponding to the expression: intensity $= 1 - 0.7 \ln$(frame number). We have found that the same logarithmic behaviour is followed by experimental data from different targets in different telescopes, although coefficients may change slightly. If we calculate the standard deviation value of the peak intensities following this exponential behaviour, we always obtain a value slightly less than one-tenth of the average intensity. Fig. 1 also shows the normalized intensity of a pixel in the halo region throughout the cube frame series, which varies randomly. If the peak intensity of the host star has this logarithmic behaviour, the peak intensity of any faint companion surrounding the host star will have the same behaviour. The central peak of a companion therefore follows the behaviour shown in Fig. 1 (black line), although its height would be much lower than that of the host star.

2.2 Halo intensity behaviour

To apply frame selection in the LI technique successfully, we need a coherent peak approximately twice the height of the surrounding speckles. This is possible only when the condition $D/r_0 < 8$ is fulfilled. In these conditions, the field in the halo area will consist of the sum of a constant phasor plus a series of random phasors with phase uniformly distributed in the interval $(-\pi, \pi)$. The probability density function of the intensity is a modified Rician density function given by (Goodman 2007):

$$p(I) = \left(\frac{1}{\bar{I}_n}\right) \exp\left(-\frac{I}{\bar{I}_n} - r\right) \boldsymbol{I_0}\left(2\sqrt{\frac{I}{\bar{I}_n}r}\right), \tag{1}$$

where $\boldsymbol{I_0}(.)$ is the zero-order modified Bessel function of the first kind, $\bar{I}_n$ represents the average intensity of the random phasor sum alone, $r = I_0/\bar{I}_n$ and I_0 is the intensity of the constant phasor alone.

The expression for the first moment is:

$$\bar{I} = (1 + r)\bar{I}_n \tag{2}$$

The STD and the signal-to-noise ratio are given by:

$$\sigma = \bar{I}_n\sqrt{1 + 2r} \tag{3}$$

and

$$\frac{S}{N} = \frac{\bar{I}}{\sigma} = \frac{1 + r}{\sqrt{1 + 2r}}. \tag{4}$$

To characterize the halo speckle we have to determine the value of the parameter r. However, the ratio between coherent and incoherent energy changes across the image plane, and it is not possible to get a single value of r. Nevertheless, if we want to estimate equation (4) it is necessary to have a good estimate of the experimental STD. A similar situation where a constant phasor is added to a series of random ones can also be found in partial adaptive optics. In this case, it has been experimentally checked (Canales & Cagigal 1999; Fitzgerald & Graham 2006) that a Rician distribution describes the speckle behaviour as well.

3 INTENSITY STATISTICS INSIDE THE HALO AREA

The light intensity within the halo area due to the host star is given by the addition of the Airy pattern plus the speckle intensity. However, in those pixels where there is a companion, we have to add the corresponding companion Airy pattern. In each pixel of the scientific camera we will therefore detect a combination of coherent and incoherent light, so that the relative weight will vary from one pixel to the next. To estimate the intensity variance in the halo area we will use the following expression:

$$\mathrm{var}\,(I_\mathrm{S} + I_\mathrm{C}) = \mathrm{var}\,(I_\mathrm{S}) + \mathrm{var}\,(I_\mathrm{C}) + 2\,\mathrm{cov}\,(I_\mathrm{S}, I_\mathrm{C}), \tag{5}$$

where I_S stands for star intensity and I_C for companion intensity. According to the experimental behaviour shown in Section 2.1, we can approximate the variance of the companion coherent peak as:

$$\mathrm{var}\,(I_\mathrm{C}) \approx \left(\frac{\bar{I}_\mathrm{C}}{10}\right)^2. \tag{6}$$

In addition, according to equations (2) and (3) the variance of the star intensity is given by:

$$\mathrm{var}\,(I_\mathrm{S}) = \bar{I}_\mathrm{S}^2\frac{1 + 2r}{(1 + r)^2}. \tag{7}$$

Now, we have to estimate the term $\mathrm{cov}(I_\mathrm{S}, I_\mathrm{C})$. The first point is that coherent and incoherent energies fluctuate in counter phase, so the sign of the covariance should be negative. However, speckle intensity fluctuations are independent of the star's intensity fluctuations, as can be seen in the blue line of Fig. 1. Experimental estimates of the covariance confirm this fact and provide covariance values that are negligible compared to variances given by equations (6) and (7):

$$\mathrm{cov}\,(I_\mathrm{S}, I_\mathrm{C}) \approx 0 \tag{8}$$

The pixel intensity STD will therefore be:

$$\sigma\,(I_\mathrm{S} + I_\mathrm{C}) \approx \sqrt{\left(\frac{\bar{I}_\mathrm{C}}{10}\right)^2 + \bar{I}_\mathrm{S}^2\frac{1 + 2r}{(1 + r)^2}}. \tag{9}$$

According to equation (9), in those pixels with only incoherent energy, the STD will correspond to that of speckled light. However, in those pixels containing a companion, the STD has an extra

component, which depends on its coherent intensity. The SNR is given by:

$$\frac{S}{N} = \frac{\bar{I}_S + \bar{I}_C}{\sqrt{\left(\frac{\bar{I}_C}{10}\right)^2 + \bar{I}_S^2 \frac{1+2r}{(1+r)^2}}}, \tag{10}$$

which, in those pixels where there is no companion ($I_C = 0$), coincides with that of equation (4).

4 EXPERIMENTAL DATA

Ginski et al. (2016) published images obtained using the 2.2 m telescope at CAHA (Almería, Spain) of a series of newly detected comoving companions of exoplanet host stars. We draw attention here to Kepler-21, which exhibits a comoving companion, Kepler-21b, which is located about 0.8 arcsec south-east of the host star and whose intensity is about 100 times fainter than the host star. The observations were carried out using Astralux. This instrument incorporates a fast readout electron multiplying CCD chip (EMCCD) which is able to acquire images with a very low readout noise. Astralux allows the acquisition of a large number of images, typically several thousand for each target, with exposure times of about a few tens of ms, which allows us to freeze atmospheric speckles. Conventional long integration time averages these speckles to produce a seeing-limited point spread function. The observations were done in the SDSS *I*-band with a pixel scale of 47 marcsec pixel^{-1}. 50 000 images were acquired, each with an exposure time of about 30 ms. With standard LI techniques and high-pass filtering, the companion was recovered with a signal-to-noise ratio of about SNR = 1.6, using the best 1 per cent of all images of the star. In this paper, we use a cube of 500 frames presenting the highest Strehl and extracted from those measured by Ginski et al. (2016). This set of images was used to assess the effect of different techniques on the target SNR.

5 ESTIMATE PROCEDURES

A good STD estimate is crucial for knowing the behaviour of the halo, and there are two different options for estimating it. The first option is to estimate the STD of the intensity for a particular pixel throughout the LI cube. This is a kind of temporal estimate and it has the advantage of presenting a high spatial resolution since only one pixel is involved in the estimate. We use σ_t to designate the frame containing the set of temporal STD obtained throughout an LI cube. However, as the star intensity decreases throughout the LI cube (Fig. 1), the mean value of the halo intensity increases. This is a case of heteroscedasticity and the temporal estimate σ_t does not take this into account. The second option is to estimate the STD in an area around a particular pixel. The result of this procedure is a cube of frames containing the spatial STD estimate from each frame. We call this $C\sigma_e$. The series $C\sigma_e$ can also be averaged to produce a frame containing the average spatial STD, σ_e. In the case of the spatial estimate, the choice of the area used to estimate the STD could be significant. A small area, for example 3×3 pixels, does not contain a number of samples high enough to achieve a good STD estimate. However, when the number of pixels of the area increases, for example to 7×7 pixels, the STD estimate is carried out on very different regions of the image and what we obtain is a kind of smoothed version of the real STD spatial distribution. The proper area size will then depend on the pixel scale of our images.

Fig. 2 shows STD estimate values throughout a line crossing the central star peak. The highest peak corresponds to σ_e, estimated in an area of 3×3 pixels (red line). When the area increases to 7×7 pixels, we obtain a kind of averaged version of the curve obtained for 3×3 pixels (black line). The temporal STD estimate, σ_t, presents a peak of about 2/3 the σ_e peak height and a wider distribution (blue line). Hence, both the height and the shape will depend on the procedure used; consequently, we have to consider this difference in future applications. The experimental STD values in Fig. 2 are theoretically described by equation (9). In general, the STD in pixels within the halo depends on the speckle statistics of the light coming from the host star. In those pixels where there is a companion, however, the STD value depends on the speckle statistics of both the host star and the companion.

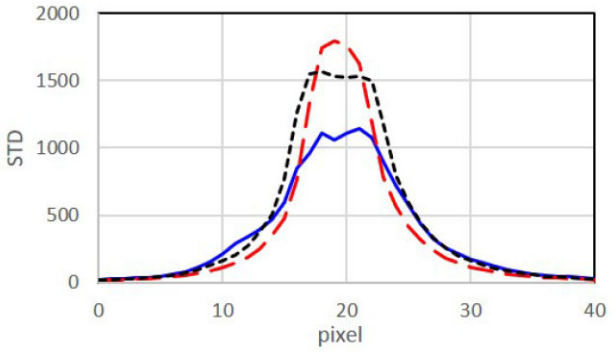

Figure 2. STD values estimated throughout the LI cube, σ_t (solid blue line), and averaged spatial estimate, σ_e, for an area of 3×3 pixels (dashed red line) and 7×7 pixels (dotted black line). The halo radius given by λ/r_0 is 19 pixels.

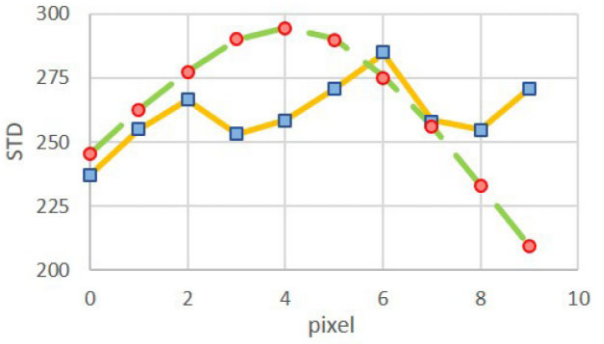

Figure 3. Averaged spatial STD, σ_e (7×7), for the original cube (red circles) and for the cube once the fake companion has been included in pixel 4 (dashed-green line). Temporal STD, σ_t, for the original cube (yellow line) and for the cube once the fake companion has been included (blue squares).

To check the effect of companion coherent light in the STD of the halo, we have introduced a fake companion within the halo area. We have taken an experimental LI cube of frames, displaced it at a distance corresponding to the third Airy ring and divided the cube intensity by 300. The companion intensity is therefore about four times greater than the coherent light corresponding to the third Airy ring where it is located. The resulting cube has been added to the original one. We then calculated in Fig. 3 the averaged spatial STD, σ_e (7×7), for the original cube (red line) and for the cube containing the fake companion (dashed green line). The curves show that the presence of this particular companion has not produced any significant variation in the spatial STD curve. We repeated the process this time evaluating the temporal STD, σ_t, along the same line profile and we obtained the corresponding curves without (blue line) and with (dashed yellow line) a companion. Once again, the introduction

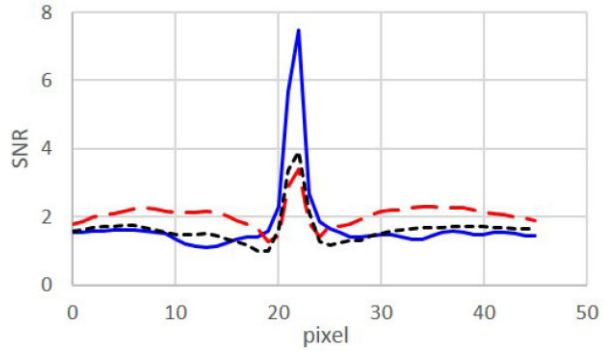

Figure 4. SNR estimate throughout a line crossing the peak star (pixel 22) using the temporal STD estimate σ_t (blue line) and the spatial STD estimate σ_e (3×3) (dashed red line) and σ_e (7×7) (dotted black line).

of the companion does not produce any significant change in the value of σ_t. We may conclude, then, that, except for very bright companions, both the σ_e and σ_t values come from the halo intensity fluctuations as described by equation (9). Finally, we can also see that STD values are similar in both cases, but that the σ_t values may present important changes from point to point whilst σ_e values are a kind of local average of the STD values.

6 DETERMINATION OF THE *r* PARAMETER

Once we know how to estimate the different types of STD, we can estimate the SNR of equation (4). Fig. 4 shows the SNR estimated using the temporal STD estimate σ_t (blue line), the spatial STD estimate σ_e (3×3) (dashed red line), and the spatial STD estimate σ_e (7×7) (dotted black line) through a line crossing the star peak. In all cases, there is a central area with radius of about 3 pixels, where the coherent light exceeds the incoherent light; consequently, the variance is given by equation (6). Outside this area, the SNR remains approximately stable with a value around 1.6 for the temporal σ_t estimate and for the spatial σ_e (7×7) estimate. The SNR for the spatial σ_e (3×3) presents a shorter central peak and a value greater than 2 in the halo area.

To understand this difference, we have to bear in mind that the experimental STD estimate only gives us an STD value which is affected by different errors and whose magnitude will depend on the procedure followed. The poor quality of the σ_e (3×3) estimate is due to the use of only nine samples for its evaluation. On the other hand, when we use σ_e (7×7), the number of samples used to estimate the spatial STD increases to 49, which reduces the noise in the STD estimate. However, this estimate corresponds to the STD averaged over different regions of the halo. Finally, the temporal STD estimate is affected not only by the halo intensity fluctuations but also by an increase of the mean halo intensity throughout the cube, as shown in Fig. 1. Nevertheless, if we consider the SNR in the halo to be about 1.6, and use equation (4), we obtain $r \approx 3$.

To check the experimental behaviour of the pixels intensity, we have selected a pixel located in the halo and calculated the intensity histogram throughout the cube. Fig. 5 shows the number of times a particular intensity appears in the cube (blue line). Once we know that $r \approx 3$ and we measure the mean intensity, we can calculate the $p(I)$ from equation (1). We see that experimental statistics fit with what is theoretically expected from equation (1) (red line in Fig. 5) for the pixel mean intensity of this particular pixel position and $r \approx 3$.

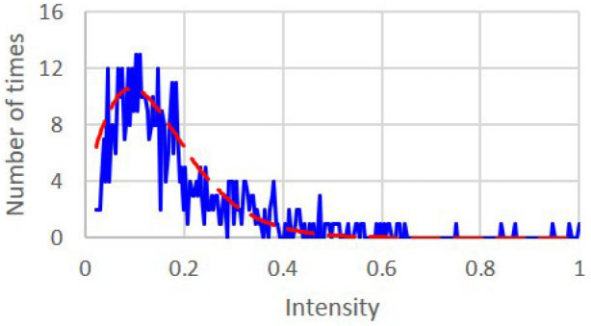

Figure 5. Experimental (blue line) and theoretical (dashed-red line) intensity statistics.

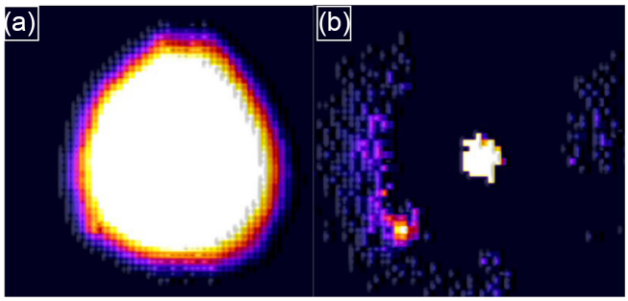

Figure 6. (a) Experimental average intensity of Kepler-21 LI cube. (b) Experimental average intensity of the same cube after the STD subtraction. The companion Kepler-21b is now clearly visible.

7 COMPANION DETECTION PROCEDURE

We have shown in Fig. 3 that the variation of the halo STD due to the presence of additional companions is small compared to the halo STD, except for very bright ones. Therefore, the experimentally estimated STD will correspond mainly to the speckled light coming from the host star. If we have an experimental LI cube, we can estimate the STD cube, then multiply it by the *r* constant and subtract this result from the original LI cube. This will provide an LI cube where speckled halo light has been removed. The resulting image will contain the sources showing different statistics from those of the speckled halo. Fig. 6 shows the LI cube average intensity before (Fig. 6a) and after (Fig. 6b) the STD subtraction.

According to Section 6, different estimate procedures will provide different STD values. We will limit our analysis to case of the spatial STD estimate, $C\sigma_e$, since σ_t is strongly affected by the frame selection process used to create the LI cube and this can produce biased values. Besides, the temporal estimate of STD is an averaged value throughout the cube and so is not able to compensate for the heteroscedasticity that the LI cube presents. We first define the cube SLI obtained by subtracting the spatial STD cube from the LI cube. When the spatial STD is evaluated using a 7×7 mask we have:

$$\mathrm{SLI} = \mathrm{LI} - r\ C\sigma_e(7x7). \tag{11}$$

To check the effect of the subtraction of $C\sigma_e$ in the companion detection, we have introduced a fake companion in the halo area. We have taken an experimental LI cube of frames, displaced it at a distance corresponding to the third Airy ring and divided the cube intensity by 250. The companion intensity is therefore about three times greater than the coherent light corresponding to the third Airy ring where it is located. The resulting cube has been added to the original one. We applied two different techniques to detect the

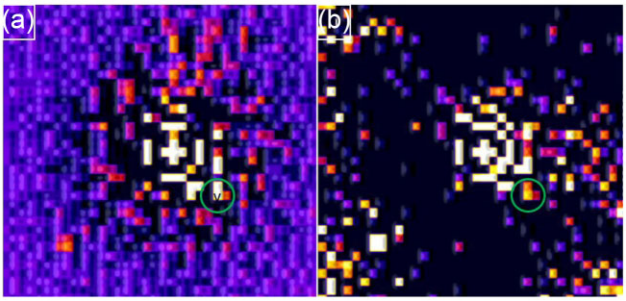

Figure 7. (a) Result of applying a Laplacian filter to the LI cube average. (b) Result of applying the COELI algorithm to the LI cube.

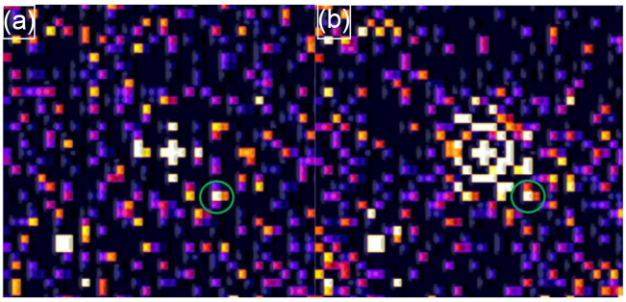

Figure 8. (a) Result of applying a Laplacian filter to the LI cube average after the subtraction of the STD cube $C\sigma_e$. (b) Result of applying the COELI algorithm to the LI cube after the subtraction of the STD cube $C\sigma_e$.

fake companion we have introduced. The first consists in applying a high-frequency (Laplacian) filter to an average image. The second technique is COELI, which has already been described (Cagigal et al. 2016, 2017). We apply the two techniques to the original LI cube and to the SLI cube defined by equation (11).

To apply the high-frequency filtering, we re-centred all the frames in the cube so that the pixel with the highest intensity is placed in the centre of each frame. We next calculate the average of the cube and apply a Laplacian filter to the resulting average image. Fig. 7(a) shows the resulting image after applying this technique to the LI cube. We can see the companion we have introduced, surrounded by a green ring, showing a low SNR (SNR ≈ 1), which is comparable to that of many other pixels around the host star. There is another already known companion placed in the lower left-hand corner presenting SNR ≈ 3. Fig. 7(b) shows the image obtained applying the algorithm COELI to the LI cube. The companion that we have introduced now shows SNR ≈ 2.3, which is higher than before and higher than that of most pixels around the star. In addition, the companion placed on the lower left-hand corner presents a value SNR ≈ 4.5.

Fig. 7 shows previously known results. Now, to see the effect of the subtraction of the cube $C\sigma_e$, we repeat the two techniques, high pass filtering and COELI, to the SLI cube. Fig. 8(a) shows the image obtained after applying a Laplacian filter to the SLI cube defined by equation (11). The fake companion is clearly visible (SNR ≈ 3.2), most of the noise having been removed and the companion in the lower left-hand corner clearly standing out against the background. Applying the COELI algorithm to the SLI cube, we obtain Fig. 8(b). The companion now shows up more clearly (SNR ≈ 4.3) and we can glimpse the two first Airy rings around the host star. The appearance of the Airy rings is a consequence of the COELI algorithm, which enhances the coherent light in the images of the cube. We see that

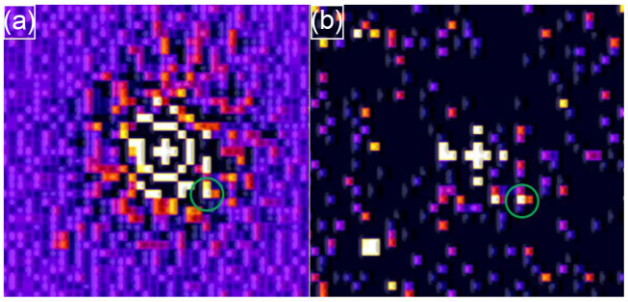

Figure 9. (a) Result of applying a Laplacian filter to the LI cube average after the division by the STD cube $C\sigma_e$. (b) Result of applying the COELI algorithm to the LI cube after the division by the STD cube $C\sigma_e$.

the subtraction of the cube $C\sigma_e$ has produced a clear improvement in image quality and increased the SNR of the companions.

8 SNR ANALYSIS

Another way to obtain information about the existence of possible companions is to analyse the SNR of the pixels in the image. To carry out this analysis, we create an SNR cube by dividing, frame by frame, the original LI cube by the STD cube $C\sigma_e$. We can then apply a Laplacian filter to the average SNR cube. The result is shown in Fig. 9(a). We can also estimate the correlation between the SNR of the central pixel and the remaining pixels by applying the COELI algorithm to the SNR cube. Fig. 9(b) shows the resulting image after applying COELI. In both cases, the companion presents a good contrast with respect to the background, although the COELI algorithm offers a much clearer image.

We see that the image obtained after the high-pass filtering of the averaged SNR cube (Fig. 9a) is similar to Fig. 7(a), which was obtained from the high-pass filtering of the averaged LI cube. In both cases, the fake companion presents a clear contrast against the background but there are many pixels showing the same contrast value. However, in Fig. 9(b) SNR ≈ 5 for the companion and the number of possible companions has dramatically dropped. We see that Fig. 9(b), which was obtained by applying COELI to the SNR cube, is very similar to Fig. 8(a), which was obtained by high-pass filtering the SLI cube defined by equation (11). The fact that two completely different techniques provide very similar images is interesting.

9 PHOTOMETRY

So far, we have focused on the developing techniques capable of detecting companions. We have not, however, paid attention to the companion photometry. It is difficult to estimate accurate photometry and even more difficult in the halo area, since the halo intensity may be much greater than the brightness of the companion. Therefore, the first step should be the removal the intensity of the halo. Since Fig. 4 gives us the ratio between the halo intensity and its STD, we calculate the temporal STD, σ_t, and multiply it by a coefficient given by Fig. 4. The coefficient will range from 1.0, for points close to the star, to 1.6 for points on the border of the halo. We then calculate the average of the recentred compensated LI cube, CLI, using the following expression:

$$\mathrm{CLI} = \langle \mathrm{LI} - \sigma_t \ \mathrm{coef} \rangle. \tag{12}$$

The second step is to binarize an image where the object of interest has a high SNR. Pixels with intensity below the object intensity

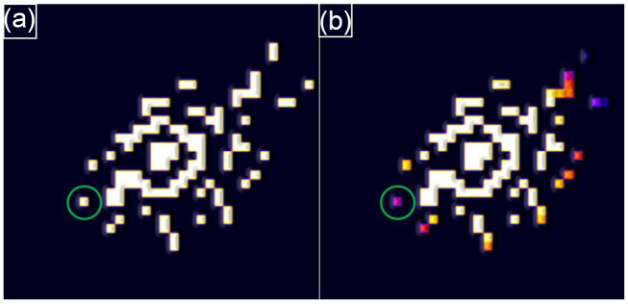

Figure 10. (a) Binary image resulting from the application of equation (13) to the experimental LI cube. (b) Correct photometry images result from multiplying Fig. 10(a) by the average of the corrected cube given by equation (12).

are set to zero and the remainder to one. We apply the binarization process to Fig. 8(a), obtained after applying a Laplacian filter to the SLI cube of equation (11):

$$\mathrm{BI} = \mathrm{Bin}\left(\mathrm{Lap}\left(\langle \mathrm{SLI} \rangle\right)\right). \tag{13}$$

Finally, we multiply the last two results to obtain the photometric image, PI:

$$\mathrm{PI} = \mathrm{CLI} \cdot \mathrm{BI} \tag{14}$$

This expression has been applied to estimate the intensity of different fake companions using cubes of different host stars from different telescopes. We have checked that the key parameter is the value of the coefficient used in equation (12) and given by Fig. 4. As an example, we apply this technique to an LI cube of 400 frames of the star FK815, which correspond to the best 10 per cent of the total number of detected frames. Images were captured by the 1.5-m Carlos Sánchez Telescope at the Teide Observatory on 2016 August 8 using FastCam. FastCam is a lucky imaging instrument, designed to perform high spatial and time resolution observations (Oscoz et al. 2008). The optics provide a plate scale of 43.5 m arcsec pixel^{-1} and a field of view of $\approx 22 \times 22$ arcsec^2. Starting from the experimental LI cube, we have followed the same steps already explained in Section 6 to introduce a fake companion placed at the position (−5,5) with respect to the host star and with an intensity 150 times lower than that of the host star. Fig. 10(a) shows the binary image resulting after applying equation (13).

In this case, the SLI cube, was obtained according to equation (11) but we used a 3×3 mask to estimate the spatial STD. The compensated image was calculated according to equation (12) and the coefficient value used was 1.4. After the product given by equation (14), we obtain the image shown in Fig. 10(b). If we calculate the ratio between the host star and companion intensity we obtain a value about 200. This means that the procedure estimates the relative intensity of the companion with an error of about 35 per cent. Applying this procedure to other experimental LI cubes, we have found errors in the companion intensity estimate of up to 50 per cent. However, the error in the companion intensity estimate will strongly depend on the right estimate of the coefficient value appearing in equation (14).

10 CONCLUSIONS

We have shown that in lucky imaging the statistics of the speckle light in the halo surrounding a star can be described by a modified Rician distribution. Under these conditions, there is a relationship between the halo height and its STD. We removed the halo by subtracting from the LI cube the cube of local STD values multiplied by a factor, and we call this the SLI cube. This allows us to compensate for the heteroscedasticity of the LI cube and, at the same time, reduce the speckled halo around the host star. We applied two techniques, high-pass filtering and COELI algorithm, to process the LI cube and the SLI cube and compared the results. We found that the SNR of a companion increased by a factor of around 3 for the high-pass filtering and a factor of 2 for COELI when the LI cube was replaced by the SLI cube. Since the STD depends on the nature of the object producing the signal, we created the SNR cube by dividing the LI cube by the STD cube frame by frame. The SNR cube was also processed by both techniques. We obtained good results, the companion SNR increasing to 5 for COELI processing. So far, the techniques introduced have been effective in detecting companions but the resulting image did not give any idea of the relative brightness of the objects. Finally, we developed a technique to get a rough estimate of the companion intensity that provides good results, with errors below 50 per cent, but that is very sensitive to the parameters used in the estimating process.

ACKNOWLEDGEMENTS

Funding by Ministerio de Economía y Competitividad, project AYA2016-78773-C2-1-P.

DATA AVAILABILITY

Data underlying the results presented in this paper are not publicly available at this time but may be obtained from the authors upon reasonable request.

REFERENCES

Cagigal M. P., Valle P. J., Colodro-Conde C., Villo-Perez I., Perez-Garrido A., 2016, MNRAS, 455, 2765
Cagigal M. P., Valle P. J., Cagigas M. A., Villo-Perez I., Colodro-Conde C., Ginski C., Mugrauer M., Seeliger M., 2017, MNRAS, 464, 680
Canales V. F., Cagigal M. P., 1999, Appl. Opt., 38, 766
Fitzgerald M. P., Graham J. R., 2006, ApJ, 637, 541
Fried D. L., 1978, J. Opt. Soc. Am., 68, 1651
Ginski C. et al., 2016, MNRAS, 457, 2173
Goodman J. W., 2007, Speckle Phenomena in Optics. Roberts and Company Publishers, Greenwood Village, CO, p. 31
Hardy J. W, 1998, Adaptive Optics for Astronomical Telescopes. Oxford Univ. Press, Oxford
Hormuth F., Hippler S., Brandner W., Wagner K., Henning T., 2008, in McLean I. S., Casali M. M., eds, Proc. SPIE Conf. Ser. Vol. 7014, Ground-based and Airborne Instrumentation for Astronomy II. SPIE, Bellingham, p. 48
Mackay C., 2013, MNRAS, 432, 702
Oscoz A. et al., 2008, in McLean I. S., Casali M. M., eds, Proc. SPIE Conf. Ser. Vol. 7014, Ground-based and Airborne Instrumentation for Astronomy II . SPIE, Bellingham, p. 48
Weigelt G., Wirnitzer B., 1983, Opt. Lett., 8, 389

This paper has been typeset from a TEX/LATEX file prepared by the author.